J Biomol NMR (2011) 51:71–82
DOI 10.1007/s10858-011-9542-0

ARTICLE

Active site dynamics in NADH oxidase from *Thermus thermophilus* studied by NMR spin relaxation

Teresa Miletti · Patrick J. Farber · Anthony Mittermaier

Received: 5 May 2011 / Accepted: 28 June 2011

Abstract We have characterized the backbone dynamics of NADH oxidase from *Thermus thermophilus* (NOX) using a recently-developed suite of NMR experiments designed to isolate exchange broadening, together with ^{15}N R_1, $R_{1\rho}$, and $\{^1H\}$-^{15}N steady-state NOE relaxation measurements performed at 11.7 and 18.8 *T*. NOX is a 54 kDa homodimeric enzyme that belongs to a family of structurally homologous flavin reductases and nitroreductases with many potential biotechnology applications. Prior studies have suggested that flexibility is involved in the catalytic mechanism of the enzyme. The active site residue W47 was previously identified as being particularly important, as its level of solvent exposure correlates with enzyme activity, and it was observed to undergo "gating" motions in computer simulations. The NMR data are consistent with these findings. Signals from W47 are dynamically broadened beyond detection and several other residues in the active site have significant R_{ex} contributions to transverse relaxation rates. In addition, the backbone of S193, whose side chain hydroxyl proton hydrogen bonds directly with the FMN cofactor, exhibits extensive mobility on the ns–ps timescale. We hypothesize that these motions may facilitate structural rearrangements of the active site that allow NOX to accept both FMN and FAD as cofactors.

Keywords Protein dynamics · NMR spin relaxation · NADH oxidase · Catalytic mechanism

T. Miletti · P. J. Farber · A. Mittermaier (✉)
Department of Chemistry, McGill University, Montreal, QC H3A 2K6, Canada
e-mail: anthony.mittermaier@mcgill.ca

Introduction

NADH oxidase (NOX) from the thermophilic bacterium *Thermus thermophilus* catalyzes the oxidation of NADH and NADPH to NAD^+ and $NADP^+$, with the concomitant reduction of O_2 to H_2O_2. Although the biological function of NOX is unclear, the enzyme is of interest as a component of dehydrogenase-based biosensors (Serban and El Murr 2006). In addition, NOX belongs to a family of structurally homologous flavin reductases and nitroreductases that includes enzymes with applications in gene therapy (Dachs et al. 2005; Palmer et al. 2005) and environmental remediation (Best et al. 2005; Kurumata et al. 2005). The enzyme is a symmetric homodimer of 205 amino-acid monomers and binds two FMN or FAD cofactors in active sites formed between the subunits (Hecht et al. 1995). Catalysis follows a ping-pong mechanism in which a bound FMN or FAD molecule is first reduced to $FMNH_2$ or $FADH_2$ via two-electron transfer from NADH. The oxidised cofactor is then regenerated by O_2, external flavin, or a variety of other electron acceptors including ferricyanide (Zoldak et al. 2003) and hydroxymethyl ferrocene (Serban and El Murr 2006). The enzyme is most active at about 70°C, near the physiological temperature of *Thermus thermophilus*. The value of k_{cat} is roughly twofold lower at 50°C and tenfold lower at 20°C, compared to 70°C.

Protein flexibility is believed to play a key role in the catalytic cycle of NOX. The addition of low concentrations (approx. 1 M) of urea (Zoldak et al. 2003) and other chaotropic agents (Zoldak et al. 2004) increase both k_{cat} and K_m by up to 2.5-fold at 20°C. This modulation of catalysis is accompanied by structural and dynamical changes in the enzyme that involve increased solvent exposure of an active-site tryptophan, W47, as indicated by fluorescence

quenching experiments (Zoldak et al. 2003, 2004). Higher concentrations (approx. 6 M) of urea inactivate the enzyme. Conversely, the addition of SO_4^{2-} and other kosmotropes lead to reduced k_{cat} and K_m values and reduced solvent exposure of W47 (Zoldak et al. 2004). Some information on the nature of active-site dynamics was provided by computer simulations that showed the side chain of W47 undergoing large-amplitude excursions that could influence the ability of the substrate to gain access to the cofactor.

In order to better understand the role of protein dynamics in the mechanism of this enzyme, we have used NMR spin relaxation experiments to characterize ms–μs and ns–ps timescale backbone motions of NOX. We employed a combination of standard ^{15}N R_1, R_2, and $^1H/^{15}N$ steady-state NOE experiments and a recently-developed suite of pulse sequences that measures the decay of longitudinal two-spin order and single-quantum and multiple-quantum coherences (referred to here as LOSMQ experiments). The experiments yield both exchange-free ^{15}N transverse relaxation rates and estimates of the exchange-broadening contributions to ^{15}N $R_{1\rho}$ values (Hansen et al. 2007, 2009). Residues exhibiting enhanced flexibility on both the ms–μs and ns–ps timescales cluster near the FMN cofactor in the active site of the enzyme. Notably W47, which was previously implicated in active-site dynamics, does not produce detectable signals in NMR spectra, suggesting that this residue experiences extensive dynamical broadening. Large exchange contributions to transverse relaxation rates are seen for several other residues in the active site. In addition, a region of the protein that directly contacts the FMN cofactor exhibits a high degree of mobility on the ns–ps timescale. These results support the idea that the NOX active site is conformationally flexible, and shed some light on the complex array of internal motions that it experiences.

Materials and methods

Protein production

^{15}N and $^{15}N/^{13}C$-enriched protein samples were prepared as described previously (Marley et al. 2001). Briefly, *E. coli* bacteria (NovaBlue, EMD Biosciences, San Diego CA, USA) were transformed with plasmid encoding *T. thermophilus* NOX under the control of a *tac* promoter (Park et al. 1992). Bacteria were grown at 37°C in 2 l of LB broth to an OD_{600} of 0.7, pelleted by centrifugation and resuspended in 500 ml of M9 minimal media with $^{13}C/^1H$ glucose and/or $^{15}NH_4Cl$ (Sigma-Aldrich, St. Louis MO, USA) as the sole carbon and/or nitrogen source. Expression was induced 1 h after transfer through the addition of 200 mg/ml isopropyl b-D-thiogalactoside (IPTG, EMD Biosciences, San Diego CA, USA). Bacteria were harvested by centrifugation after 6 h of incubation.

Samples enriched in ^{15}N, ^{13}C, and ^2H were prepared according to the following protocol. A starter culture of *E. coli*, transformed with the NOX plasmid, was grown in M9 minimal media at 37°C without isotopic enrichment. Upon reaching an OD_{600} of 0.7, the cells were pelleted by centrifugation and re-suspended in M9 minimal media containing 90% D_2O and $^{13}C/^1H$ glucose and $^{15}NH_4Cl$ (Sigma-Aldrich, St. Louis MO, USA) to give an initial OD_{600} of approximately 0.10. Expression was induced when the OD_{600} reached 0.7, as above. Bacteria were harvested by centrifugation after 20 h of incubation at 37°C.

Cells were resuspended in a buffer containing 50 mM Tris–HCl, 5 mM benzamidine, 2 mM ethylenediaminetetraacetic acid (EDTA), pH 7.5, disrupted by sonication, and the insoluble material was separated by centrifugation. The supernatant was incubated at 80°C for 5 min, causing most native *E. coli* proteins to precipitate while leaving the thermophilic NOX in solution (Park et al. 1992), and cleared by centrifugation. The supernatant was then passed through a DEAE ion-exchange column, which bound many of the contaminants, but did not bind NOX. The pH was reduced to 5.0 through the addition of 50 mM acetate buffer. NOX was purified by cation exchange chromatography using SP-Sepharose resin followed by size-exclusion chromatography using a HiLoad 16/60 Superdex 75 FPLC column (GE Healthcare, Little Chalfont, UK). NMR samples contained between 0.8 and 1 mM NOX (monomer concentration), 50 mM potassium phosphate pH 7.2, 2.4 mM riboflavin 5′-monophosphate (FMN, Sigma-Aldrich, St. Louis MO, USA), 5% D_2O and 10 μM 2,2-dimethyl-2-silapentane-5-sulfonate (DSS, Sigma-Aldrich, St. Louis MO, USA) as an internal chemical shift reference. These sample conditions were chosen to coincide with those used previously for enzymatic activity assays (Zoldak et al. 2003).

NMR spectroscopy

NMR data were recorded at 50°C using Varian INOVA spectrometers equipped with cold probes operating at ^1H Larmor frequencies of 500 MHz (11.7 *T*) and 800 MHz (18.8 *T*). Backbone assignments were obtained using $^{15}N/^{13}C$ and $^{15}N/^{13}C/^2H$ labelled samples and HNCA, HNCO (Ikura et al. 1990), HN(CO)CA, HN(CA)CO (Yamazaki et al. 1994), HNCACB (Wittekind and Mueller 1993), CBCA(CO)NH (Grzesiek and Bax 1992) and NOESY (Zhang et al. 1994) experiments performed at 18.8 *T*. The data were processed using the NMRPipe/NMRDraw (Delaglio et al. 1995) suite of programs and analyzed using NMRView (Johnson and Blevins 1994).

^{15}N R_1 (Farrow et al. 1994) and $R_{1\rho}$ (Korzhnev et al. 2002) relaxation rates were measured at 11.7 T and 18.8 T for an ^{15}N-enriched protein sample. The temperatures on both instruments were calibrated using a methanol reference (Amman et al. 1982). The R_1 experiments employed relaxation delays of 0.0334, 0.0668, 0.111, 0.145, 0.189, 0.234, 0.289, 0.345, 0.412, 0.479, 0.557 s (11.7 T) and 0.0109, 0.0981, 0.196, 0.316, 0.425, 0.556, 0.687, 0.840, 1.01, 1.20, 1.40, 1.64 s (18.8 T). The $R_{1\rho}$ experiments employed relaxation delays of 0.01, 0.02, 0.03, 0.04, 0.05, 0.06, 0.07, 0.08, 0.09, 0.1 s and spin-lock fields of 1.5 kHz at both 11.7 T and 18.8 T. Relaxation rates were determined by non-linear least-squares fitting of the peak intensities to the exponential decay function,

$$I(T_{relax}) = I_0 \cdot \exp(-RT_{relax}), \tag{1}$$

where T_{relax} is the delay time, I_0 is the initial peak intensity and R is the relaxation rate. Uncertainties in R_1 and $R_{1\rho}$ were estimated from the deviations between experimental peak intensities and their back-calculated values. R_2 values were calculated from experimental R_1 and $R_{1\rho}$ measurements according to the expression

$$R_2 = \frac{R_{1\rho} - R_1 \cos^2\theta}{\sin^2\theta} \tag{2}$$

where

$$\theta = \tan^{-1}(\nu_{SL}/\Delta\nu), \tag{3}$$

$\Delta\nu$ is the offset of the peak from the carrier frequency and ν_{SL} is the strength of the spin lock, in Hz. $\{^1\text{H}\}^{15}$N steady-state NOE values were calculated as the ratio of peak volumes obtained with 5 s of proton presaturation and a 7 s interscan delay, relative to those obtained with no proton saturation and a 12-s interscan delay. Uncertainties were obtained from noise level estimates in NMRDraw.

Spectral density mapping

In order to test the consistency of relaxation rates obtained at 11.7 T and 18.8 T, data for each field strength were analyzed separately using reduced spectral density mapping (Farrow et al. 1995) to yield values of the spectral density function, $J(\omega)$, at $\omega = 0$, ω_N, and $0.87\omega_H$ (ω_N and ω_H are the ^{15}N and ^{1}H Larmor frequencies, respectively) (Morin and Gagne 2009). The values of $J(0.87\omega_H)$ were calculated according to the expression

$$J(0.87\omega_H) = \frac{4}{5d_{HN}^2}\frac{\gamma_N}{\gamma_H}(NOE - 1)R_1, \tag{4}$$

where $d_{HN} = (\mu_0/4\pi)\hbar\gamma_H\gamma_N\langle r_{NH}^{-3}\rangle$, μ_0 is the permeability of free space, $\hbar$ is the reduced Planck's constant, γ_N and γ_H are the gyromagnetic ratios of ^{15}N and ^{1}H, r_{NH} is the NH bond length, and angled brackets indicate the time average. The value of $J(\omega_N)$ was calculated according to

$$J(\omega_N) = \frac{R_1 - \frac{7}{4}d_{HN}^2 J(0.921\omega_H)}{(\frac{3}{4}d_{HN}^2 + c_N^2)}, \tag{5}$$

where $c_N = B_0\gamma_N\Delta\sigma_N((1 + \eta^2/3)/3)^{1/2}$, B_0 is the spectrometer magnetic field strength, $\Delta\sigma_N = \sigma_{11} - (\sigma_{22} + \sigma_{33})/2$, ($\sigma_{11}$, σ_{22}, σ_{33}) are the principle components of the ^{15}N chemical shift anisotropy tensor, $\eta = (\sigma_{22} - \sigma_{33})/(\sigma_{11} - \sigma_{iso})$, and $\sigma_{iso} = (\sigma_{11} + \sigma_{22} + \sigma_{33})/3$. The value of $J(0)$ was obtained using the expression

$$J(0) = \frac{R_2 - \frac{1}{8}d_{HN}^2(3J(\omega_N) + 13J(0.955\omega_H)) - \frac{1}{2}c_N^2 J(\omega_N)}{\frac{1}{2}d_{HN}^2 + \frac{2}{3}c_N^2} \tag{6}$$

Lower bounds for $J(\omega_N)$ and $J(0)$ were obtained by assuming that $J(0.955\omega_H) = J(0.921\omega_H) = J(0.87\omega_H)$. Upper bounds were obtained by assuming that $J(\varepsilon\omega_H) = (0.870/\varepsilon)^2 J(0.870\omega_H)$, where $\varepsilon = 0.921$ or 0.955 (Farrow et al. 1995). The upper and lower estimates differed by less than 6 and 0.2% for $J(\omega_N)$ and $J(0)$, respectively, calculated using 18.8 T relaxation data.

Relaxation data obtained at multiple spectrometer field strengths can be analyzed together using a variety of methods, including spectral density mapping (Farrow et al. 1995; Peng and Wagner 1995), and the Model-Free paradigm (see below) (Lipari and Szabo 1982). In this study, we chose to combine the 11.7 T and 18.8 T data sets using the Model-Free approach, since it explicitly separates the effects of internal motions from those of anisotropic rotational diffusion, and we find the extracted Model-Free parameters to be more intuitive than spectral density values.

Model free analysis

According to the Lipari-Szabo Model-Free approach, the spectral density function for a bond vector undergoing internal motions within a molecule in solution is given by (Lipari and Szabo 1982):

$$J(\omega) = \frac{2}{5}\left(S^2\frac{\tau_M}{1 + (\omega\tau_M)^2} + (1 - S^2)\frac{\tau}{1 + (\omega\tau)^2}\right),$$
$$\tau^{-1} = \tau_M^{-1} + \tau_e^{-1} \tag{7}$$

where S^2 and τ_e are the order parameter and correlation time describing the amplitude and timescale of bond vector internal dynamics, respectively, and τ_M is the effective correlation time for molecular tumbling in solution. In the quadric approximation (Brüschweiler et al. 1995; Lee et al. 1997), the effective tumbling correlation time, τ_M, is related to the rotational diffusion tensor and the orientation of each bond vector in the molecular frame by the

following expressions:In the case of fully anisotropic tumbling,

$$\left(6\tau_{M,i}\right)^{-1} = e_i^T \mathbf{A}^{-1}\mathbf{Q}\mathbf{A}e_i \tag{8}$$

where $e_i^T = [x_i, y_i, z_i]$ are the direction cosines defined by the orientation of the ith bond vector in an arbitrary reference frame (given by the PDB coordinates), $\mathbf{A}$ rotates e_i into the principal axis frame of the diffusion tensor,

$$\begin{aligned}\mathbf{A} &= \mathbf{R_z}(\gamma)\mathbf{R_y}(\beta)\mathbf{R_z}(\alpha)\\ &= \begin{bmatrix}\cos\gamma & -\sin\gamma & 0\\ \sin\gamma & \cos\gamma & 0\\ 0 & 0 & 1\end{bmatrix}\begin{bmatrix}\cos\beta & 0 & \sin\beta\\ 0 & 1 & 0\\ -\sin\beta & 0 & \cos\beta\end{bmatrix}\\ &\quad\begin{bmatrix}\cos\alpha & -\sin\alpha & 0\\ \sin\alpha & \cos\alpha & 0\\ 0 & 0 & 1\end{bmatrix},\end{aligned} \tag{9}$$

and α, β, and γ are Euler angles for the rotation. In its principal axis frame, the diffusion tensor is given by

$$\mathbf{D} = \begin{bmatrix}D_{xx} & 0 & 0\\ 0 & D_{yy} & 0\\ 0 & 0 & D_{zz}\end{bmatrix}, \tag{10}$$

While $\mathbf{Q}$ is given by the expression

$$\mathbf{Q} = \frac{1}{2}\begin{bmatrix}D_{yy}+D_{zz} & 0 & 0\\ 0 & D_{xx}+D_{zz} & 0\\ 0 & 0 & D_{xx}+D_{yy}\end{bmatrix}. \tag{11}$$

In the case of axially symmetric tumbling, this simplifies to

$$\left(6\tau_{M,i}\right)^{-1} = \frac{1}{2}\left(D_\perp + \mathrm{D}_{||} + \left(D_\perp - \mathrm{D}_{||}\right)\left(a_{31}x_i + a_{32}y_i + a_{33}z_i\right)^2\right) \tag{12}$$

where $D_\perp = D_{xx} = D_{yy}$, $D_{||} = D_{zz}$, $a_{31} = \sin\theta\cos\varphi$, $a_{32} = \sin\theta\sin\varphi$, $a_{33} = \cos\theta$, and θ and φ relate the z-axis of the diffusion frame to the arbitrary molecular frame. In the case of isotropic diffusion, $D_{iso} = D_{xx} = D_{yy} = D_{zz}$ and $(6\tau_M)^{-1} = D_{iso}$.

Using the spectral densities from Eq. 7, values of the experimental relaxation rates and steady-state NOE can be calculated according to (Abragam 1961):

$$\begin{aligned}R_1 =& \frac{1}{4}d_{HN}^2\left(J(\omega_H-\omega_N)+3J(\omega_N)+6J(\omega_H+\omega_N)\right)\\ &+c_N^2 J(\omega_N)\end{aligned} \tag{13}$$

$$\begin{aligned}R_2 =& \frac{1}{8}d_{HN}^2\left(4J(0)+J(\omega_H-\omega_N)+3J(\omega_N)+6J(\omega_H)\right.\\ &\left.+6J(\omega_H+\omega_N)\right)+\frac{1}{6}c_N^2\left(3J(\omega_N)+4J(0)\right)\end{aligned} \tag{14}$$

$$NOE = 1+\frac{d_{HN}^2}{4R_1}\frac{\gamma_H}{\gamma_N}\left(6J(\omega_H+\omega_N)-J(\omega_H-\omega_N)\right) \tag{15}$$

The diffusion parameters and S^2 and τ_e values were obtained by non-linear least-squares optimization, minimizing the χ^2 parameter:

$$\chi^2 = \sum_{\text{experiments}}\sum_{\text{residues}}\frac{\left(Y_{\text{exp}}-Y_{calc}\right)^2}{\delta_Y^2}, \tag{16}$$

where the sum extends over all six experimental observables (R_1, R_2, NOE obtained at 11.7 and 18.8 T) and all 115 residues. Y_{exp} is an experimental relaxation rate or NOE value, δ_Y is the associated experimental uncertainty, and Y_{calc} is obtained using Eqs. 7–15 with the appropriate tumbling model. For a dataset of N residues, the isotropic, axially-symmetric, and anisotropic tumbling analysis have $2N+1$, $2N+4$, and $2N+6$ adjustable parameters: S^2 and τ_e for each residue plus (D_{iso}), ($D_\perp$, $D_{||}$, θ, φ), or (D_{xx}, D_{yy}, D_{zz}, α, β, γ), respectively.

The statistical significances, p, of the reductions in χ^2 afforded by the axially-symmetric tumbling model over the isotropic model, and the anisotropic tumbling model over the axially symmetric model were evaluated using F statistics according to (Vetterling et al. 1988):

$$F = \frac{\Delta\chi^2}{\Delta\nu}\frac{\nu_B}{\chi_B^2} \tag{17}$$

and

$$p = I_{\frac{\nu_B}{\nu_B+\Delta\nu\cdot F}}\left(\frac{\nu_B}{2},\frac{\Delta\nu}{2}\right) \tag{18}$$

where $\nu_{A,B}$ are the degrees of freedom for the two models under comparison and $\chi^2_{A,B}$ are the corresponding residual χ^2 values, calculated using Eq. 16, ($\nu_A > \nu_B$). $\Delta\chi^2 = \chi^2_A - \chi^2_B$ is the reduction in χ^2 afforded by adding $\Delta\nu = \nu_A - \nu_B$ additional adjustable parameters to the fit. I represents the incomplete beta function. All relaxation calculations were performed in MATLAB using in-house scripts. The tumbling in solution of NOX was modelled using HYDRONMR software (de la Torre et al. 2000), assuming that the viscosity of a 9:1 H_2O/D_2O mixture is 0.5572 cP at 50°C (Cho et al. 1999; Saksena et al. 1975). HYDRONMR first builds a primary hydrodynamic model of the protein by treating all non-hydrogen atoms as spheres whose size is specified by the atomic element radius (AER). In this case, AER = 3.1 Å was used. The surface of the protein is then represented by a shell of tangent small beads of radius σ, and a diffusion tensor is computed (Carrasco and de la Torre 1999). Calculations are repeated for different values of σ and extrapolated to $\sigma = 0$. We used 6 different values of σ (NSIG = 6) ranging from a lower limit (SIGMIN) of 1.5 Å and an upper limit (SIGMAX) of 2.0 Å.

Exchange-free relaxation rates

We employed a recently-developed suite of $^{15}N/^{1}H$ NMR relaxation experiments (Hansen et al. 2007) to estimate the extent of broadening due to microsecond-timescale

motions and to measure exchange-free transverse relaxation rates on a per-residue basis. These experiments measure the decay of longitudinal two-spin order, $R_1(2H_zN_z)$, transverse antiphase single quantum coherences, $R_{1\rho}(2H_z'N_z)$ and $R_{1\rho}(2H_zN_z')$ and multiple quantum coherences, $R_{1\rho}(2H_z'N_z')$, where we have followed the convention of Hansen et al. and used primes to indicate spin-locked nuclei. In what follows, we refer to this method as LOSMQ relaxation experiments. Measurements were taken for a $^{15}N/^{13}C/^{2}H$-enriched protein sample at 18.8 T with relaxation delays of 0.002, 0.007, 0.01, 0.021, 0.029, 0.036, 0.043, 0.05 s for all experiments, and ^{1}H and ^{15}N spin-locks of 12 and 2 kHz, respectively. ^{15}N transverse relaxation rates, R_{dd}, were obtained from single exponential fits according to Eq. 1, replacing $I(T_{relax})$ with $\beta(T_{relax})$,

$$\beta(T_{relax}) = \frac{I_{2H_z'N_z}(T_{relax}) \cdot I_{2H_zN_z'}(T_{relax})}{I_{2H_z'N_z'}(T_{relax}) \cdot I_{2H_zN_z}(T_{relax})}, \tag{19}$$

and R with $2\sin^2\theta_H\sin^2\theta_N R_{dd}$ (Hansen et al. 2007), where values of θ are given by Eq. 3, and θ_H and θ_N refer to the peak offsets from the ^{1}H and ^{15}N carrier frequencies, respectively. R_{dd} values are sensitive only to $^{15}N/^{1}H$ dipole/dipole interactions, i.e., they are free of exchange broadening contributions.

In order to estimate exchange contributions to ^{15}N $R_{1\rho}$, the experimental spin-locked relaxation rates ($R_1(2H_zN_z)$, $R_{1\rho}(2H_z'N_z)$, $R_{1\rho}(2H_zN_z')$, $R_{1\rho}(2H_z'N_z')$) were converted to pure transverse and multiple-quantum relaxation rates according to the expressions (Hansen et al. 2009)

$$R_2(2H_xN_z) = \frac{R_{1\rho}(2H_z'N_z) - R_1(2H_zN_z)\cos^2\theta_H}{\sin^2\theta_H} \tag{20}$$

$$R_2(2H_zN_x) = \frac{R_{1\rho}(2H_zN_z') - R_1(2H_zN_z)\cos^2\theta_N}{\sin^2\theta_N} \tag{21}$$

$$R_2(2H_xN_x) = \frac{R_{1\rho}(2H_z'N_z') - R_2(2H_xN_z)\sin^2\theta_H\cos^2\theta_N - R_2(2H_zN_x)\cos^2\theta_H\sin^2\theta_N - R_1(2H_zN_z)\cos^2\theta_H\cos^2\theta_N}{\sin^2\theta_H\sin^2\theta_N} \tag{22}$$

The exchange contributions to ^{15}N transverse relaxation present under spin-locked conditions were then calculated according to

$$R_{ex} = \frac{1}{2}\left\{R_1(2H_zN_z)\left(-1+\frac{4c_N^2}{3d_{HN}^2}\right) + R_2(2H_zN_x)\left(1-\frac{4c_N^2}{3d_{HN}^2}\right) + R_2(2H_xN_z)\left(-1-\frac{4c_N^2}{3d_{HN}^2}\right) + R_2(2H_xN_x)\left(1+\frac{4c_N^2}{3d_{HN}^2}\right)\right\}. \tag{23}$$

Results

Assignments

A $^{15}N/^{1}H$ HSQC correlation spectrum of NOX, saturated with FMN at 50°C, is shown in Fig. 1. Backbone assignments were obtained using standard triple-resonance experiments performed on a sample uniformly labelled with ^{15}N and ^{13}C. The enzyme is a symmetric dimer, with 190 non-proline residues per monomer, thus 190 backbone signals are expected, of which 165 were assigned. These data may be directly related to the secondary structure of the protein by analyzing the chemical shifts of C_α and C_β nuclei (Wishart and Sykes 1994). C_α nuclei tend to experience downfield shifts in α-helices and upfield shifts in β-sheets, compared to those in random-coil (unstructured) peptides. The opposite is true for C_β nuclei. The difference, $\Delta C_\alpha - \Delta C_\beta$, was calculated for each assigned residue and is plotted and in Fig. 2, where ΔC is the chemical shift in the protein subtracted from tabulated random-coil chemical shift (Wishart and Sykes 1994). Positive values are obtained in regions previously identified as α-helical in the X-ray crystal structure (Hecht et al. 1995), while negative values are obtained in β-sheet regions, as expected. Roughly 15 residues do not give rise to observable NMR signals. This could be due to rapid exchange of amide protons with the solvent or conformational dynamics on the ms to μs timescale that broaden the signals beyond detection. The unassigned residues are mostly located in loops and at the ends of helices and are clustered in the smaller "second domain" of the protein (Hecht et al. 1995) that comprises helices *E* and *F* (Fig. 3). This implicates these regions of the protein as being mobile and/or easily accessible for hydrogen exchange.

Since NOX is fairly large (54 kDa), we prepared a protein sample that was enriched in ^{15}N, ^{13}C, and ^{2}H to reduce transverse relaxation due to ^{1}H dipolar interactions (Gardner and Kay 1998). In order to collect $^{1}H/^{15}N$ correlation spectra, deuterons at amide positions that are introduced during bacterial protein expression in $^{2}H_2O$ must be exchanged for protons. In some cases, this occurs readily during protein purification in non-deuterated solutions. However, hydrogen bonding of the backbone amides can reduce the rates of *H/D* exchange by many orders of magnitude (Englander 2000). In fact, we found that some

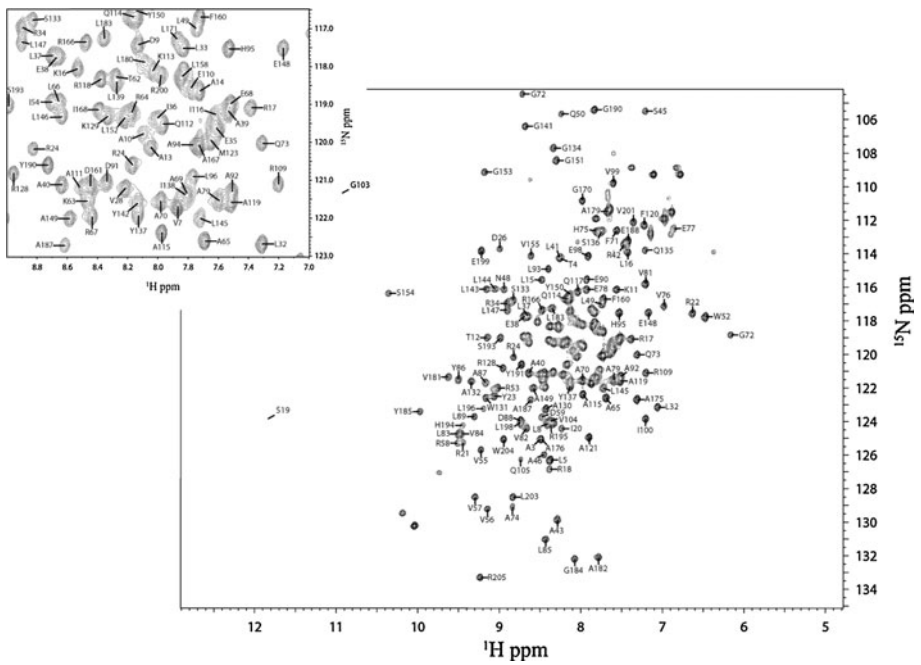

Fig. 1 Assigned HSQC spectrum of ^{15}N/^{13}C labelled NADH oxidase from *Thermus thermophilus* (NOX) recorded at 50°C and 18.8 *T* (800 MHz ^{1}H Larmor frequency)

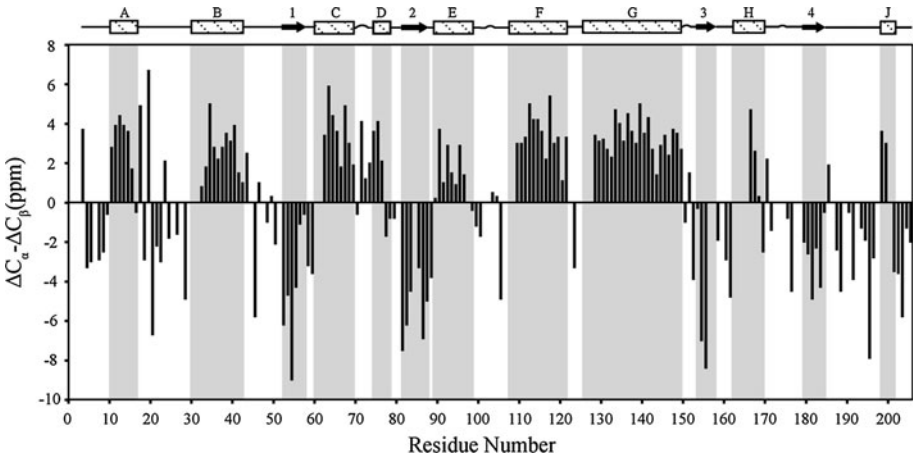

Fig. 2 Differences between ΔC_α and ΔC_β secondary chemical shifts plotted as a function of residue number. $\Delta C_{\alpha,\beta}$ is defined as the observed C_α or C_β chemical shift subtracted from the expected chemical shift of an unstructured polypeptide with the same amino acid sequence (Wishart and Sykes 1994). Positive values of ($\Delta C_\alpha - \Delta C_\beta$) are expected for α-helical residues while negative values are expected for β-sheets. Secondary structure elements were taken as (Hecht et al. 1995) α*A* (10–16), α*B* (30–42), β1 (52–57), α*C* (60–69), α*D* (74–78), β2 (81–87), α*E* (89–98), α*F* (107–121), α*G* (125–149), β3 (153–157), α*H* (162–169), β4 (179–184), α*J* (198–201)

residues in the protein interior did not exchange deuterons for protons and were not visible in HSQC spectra nor in the relaxation experiments, even after approximately 200 h of incubation at 50°C and pH 7.5. In total, there were 22 strong amide cross-peaks (with intensities within one standard deviation of the mean in the protonated sample) that remained unobservable in the deuterated sample under these conditions. We did not attempt to accelerate *H*/*D* exchange by further raising the temperature, since we have found that extended incubation at temperatures of greater than about 65°C leads to irreversible aggregation of the protein. The slow rate of *H*/*D* exchange reflects the high thermodynamic stability of the NOX structural core. Assuming that the intrinsic *H*/*D* exchange rates are on the order of 10^4 min^{-1} at 50°C and pH 7.5 (Bai et al. 1993; Connelly et al. 1993) and that less than 5% of the sample exchanged after about 200 h of incubation, the protection factors are greater than 10^9, implying that solvent-exchangeable states are at least 14 kcal/mol less stable than the ground state. This leads to a picture of NOX as an enzyme with a structurally very stable core and a more dynamic periphery (Fig. 3). Spectral assignment experiments were performed on the deuterated

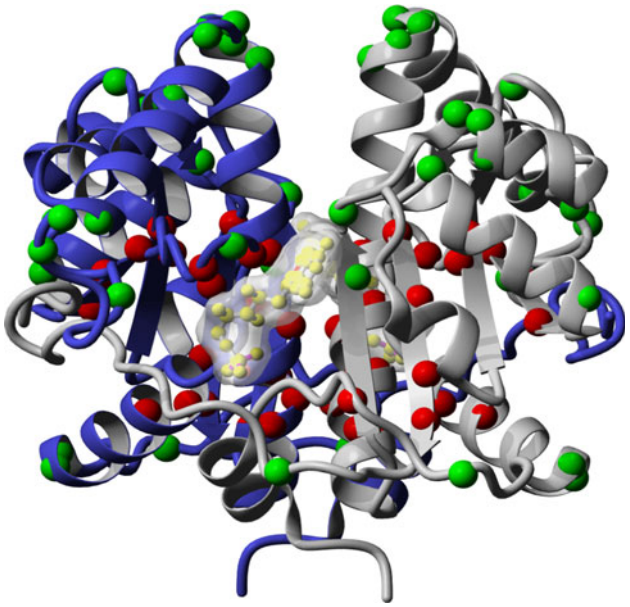

Fig. 3 Backbone ribbon diagram of NOX (Hecht et al. 1995) (PDB 1NOX), with the two subunits coloured *white* and *blue* and the FMN cofactor illustrated as *yellow balls* and *sticks* with a *semi-transparent molecular surface*. The locations of residues without assigned backbone resonances are indicated with *green spheres*. The locations of residues whose amides are highly protected from *H*/*D* exchange are indicated with *red spheres* (i.e., residues that lack signals in $^{1}H/^{15}N$ HSQC spectra of the deuterated sample after 200 h of incubation at 50°C, and whose peak intensities are greater than the mean intensity less one standard deviation in spectra of the protonated sample). Image generated with YASARA View (Krieger et al. 2002)

sample, and used to confirm the assignments obtained for the protonated enzyme.

^{15}N spin relaxation experiments

In order to probe the dynamics of NOX on the ns–ps timescale, we performed steady-state $\{^{1}H\}$-^{15}N NOE experiments (Farrow et al. 1994), and measured ^{15}N longitudinal, R_1, (Farrow et al. 1994) and rotating frame, $R_{1\rho}$, relaxation rates (Korzhnev et al. 2002), which were used to calculate pure transverse relaxation rates, R_2. Typical intensity decay curves are shown in Fig. 4. Out of 190 non-proline residues in NOX, 25 residues were not assigned and the signals for 50 residues were either overlapped or too weak to yield reliable data, leaving a relaxation data set for 115 residues. The consistency of the relaxation data was tested by calculating the value of spectral density function at zero frequency, $J(0)$, independently for measurements obtained at 11.7 and 18.8 T (Farrow et al. 1995). In the absence of exchange broadening the two data sets are expect to coincide. We found that on average, $J(0)$ values obtained at 18.8 T are 1.7% greater than those obtained at 11.7 T. This discrepancy is at the low end of values typically obtained for multiple-field relaxation data sets (Morin and Gagne 2009). The RMS deviation between the two sets of $J(0)$ values is 0.46 ns/rad, corresponding to an experimental uncertainty of about 6%.

The relaxation data obtained at 11.7 T and 18.8 T were analyzed according to the Lipari-Szabo "Model Free" formalism, in which the internal motions and the rotational diffusion of the molecule are assumed to occur independently (Lipari and Szabo 1982). In this approach, the internal reorientational dynamics of each NH bond vector are described by two parameters, S^2 and τ_e. S^2 is an order parameter that describes the magnitude of bond vector motions and can take values between 0 and 1. Bond vectors that are rigid in the molecular reference frame on the ns–ps timescale give rise to $S^2 = 1$, while those that undergo rapid unrestricted reorientation give rise to $S^2 = 0$. τ_e is the effective correlation time for NH bond vector dynamics. This combined analysis of multi-field data assumes that the protein dynamics are identical for all measurements, which requires that the sample conditions (temperature, concentration, etc.) be the same in all spectrometers used. The good agreement between $J(0)$ values calculated for the 11.7

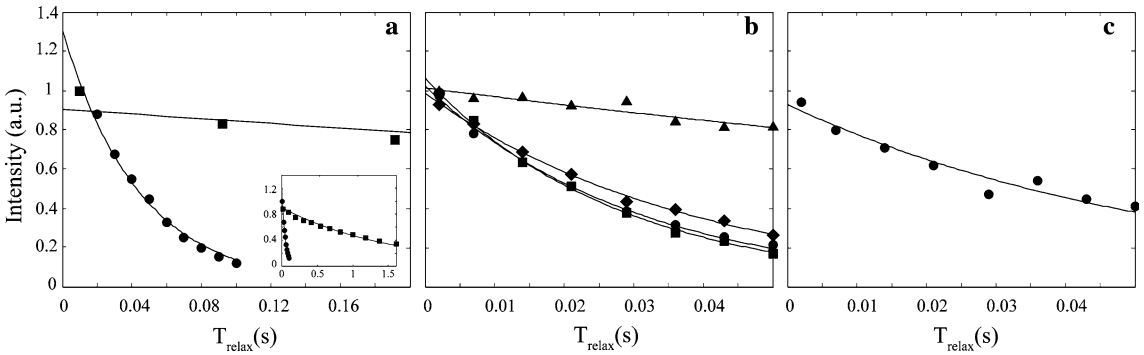

Fig. 4 Peak intensity decay curves for A121 in **a** R_1 (*squares*) and $R_{1\rho}$ (*circles*) ^{15}N relaxation experiments and **b** $2H_zN_z$ (*triangles*), $2H_z'N_z$ (*circles*), $2H_zN_z'$ (*diamonds*), and $2H_z'N_z'$ (*squares*) longitudinal order, single- and multiple-quantum (LOSMQ) relaxation experiments. Primes indicated spin-locked nuclei. **c** Decay of the $\beta(T_{relax})$ function calculated from the intensities in (**b**) according to Eq. 19

T and 18.8 *T* data sets strongly suggests that this criterion has been met (Morin and Gagne 2009).

The data were analyzed using three different models of molecular rotational diffusion (Brüschweiler et al. 1995; Lee et al. 1997). In the first model, NOX was assumed to tumble isotropically with a single rotational diffusion constant, D_{iso}. In the second model, NOX was assumed to tumble as an axially-symmetric top, such that the diagonalized diffusion tensor has two unique components, $D_{\|}$ and $D_{\perp}$ (Woessner 1962). In the third model, NOX was assumed to tumble anisotropically such that all three components of the diagonalized diffusion tensor are unique: D_{xx}, D_{yy}, and D_{zz}. In each case, the 11.7 *T* and 18.8 *T* relaxation data were analyzed simultaneously to yield separate S^2 and τ_e values for each NH bond vector and either (D_{iso}), ($D_{\|}$, $D_{\perp}$), or (D_{xx}, D_{yy}, D_{zz}). Fits using the three models had 459, 456, and 454 degrees of freedom and produced residual χ^2 values of 594, 567, and 561 for the isotropic, axially-symmetric, and anisotropic tumbling models. The improvements in fit of the axially-symmetric model over the isotropic model and the anisotropic model over the axially-symmetric model are both statistically significant, with $p = 1.5 \times 10^{-4}$ and $p = 7.9 \times 10^{-2}$, respectively. The principal components of the diffusion tensor extracted from this analysis, $D_{xx} = 0.97 \times 10^7\ s^{-1}$, $D_{yy} = 1.02 \times 10^7\ s^{-1}$, $D_{zz} = 1.11 \times 10^7\ s^{-1}$ agree quite well with those predicted using HYDRONMR software (de la Torre et al. 2000) and the X-ray crystal structure (Hecht et al. 1995), $D_{xx} = 0.95 \times 10^7\ s^{-1}$, $D_{yy} = 1.03 \times 10^7\ s^{-1}$, $D_{zz} = 1.29 \times 10^7\ s^{-1}$.

NH bond vector order parameters, S^2, extracted from the 11.7 *T* and 18.8 *T* relaxation data, assuming anisotropic rotational diffusion, are plotted as a function of residue number in Fig. 5a. Most of the values lie above 0.85, consistent with a high degree of structural rigidity. Only 7 residues gave S^2 values significantly less than 0.85 (Fig. 5). Most of these relatively flexible residues occur in loops and at the termini of α-helices and β-strands. V28 ($S^2 = 0.80 \pm 0.02$) lies in the loop connecting helices *A* and *B*. Q105 ($S^2 = 0.74 \pm 0.03$) is located in the loop between helices *E* and *F*. Interestingly, the backbone of this residue was also found to be mobile in the X-ray crystal structure (Hecht et al. 1995). The stretch of residues Q105, G106, E107 have the highest B-factors reported for the entire protein (>63 for amide *N*). W204 ($S^2 = 0.83 \pm 0.01$) lies at the extreme carboxy-terminus of the protein. Notably, a cluster of flexible residues, E188 ($S^2 = 0.77 \pm 0.01$), G190 ($S^2 = 0.80 \pm 0.02$), Y191 ($S^2 = 0.80 \pm 0.02$), and S193 ($S^2 = 0.69 \pm 0.03$) is located in a long loop that connects the fourth β-strand and the short C-terminal helix *J*, and forms part of the cofactor binding site. As discussed below, this finding suggests a possible role for ns–ps timescale motions in the catalytic mechanism of the enzyme.

Exchange-free transverse relaxation rates

We characterized NOX dynamics using a suite of NMR experiments, recently developed by Kay and co-workers, that yields ^{15}N transverse relaxation rates free from conformational exchange broadening contributions, R_{ex} (Hansen et al. 2007). Conversely, these measurements can be used to extract the R_{ex} values themselves (Hansen et al. 2009). The suite of experiments consists of single-quantum ^{15}N and ^{1}H $R_{1\rho}$ experiments, a multiple quantum experiment in which spin-locking fields are applied simultaneously to both ^{1}H and ^{15}N nuclei, and an experiment that monitors decay of longitudinal two-spin order ($2I_zS_z$ magnetization). In what follows, these will be referred to LOSMQ experiments. The linear combination of the four

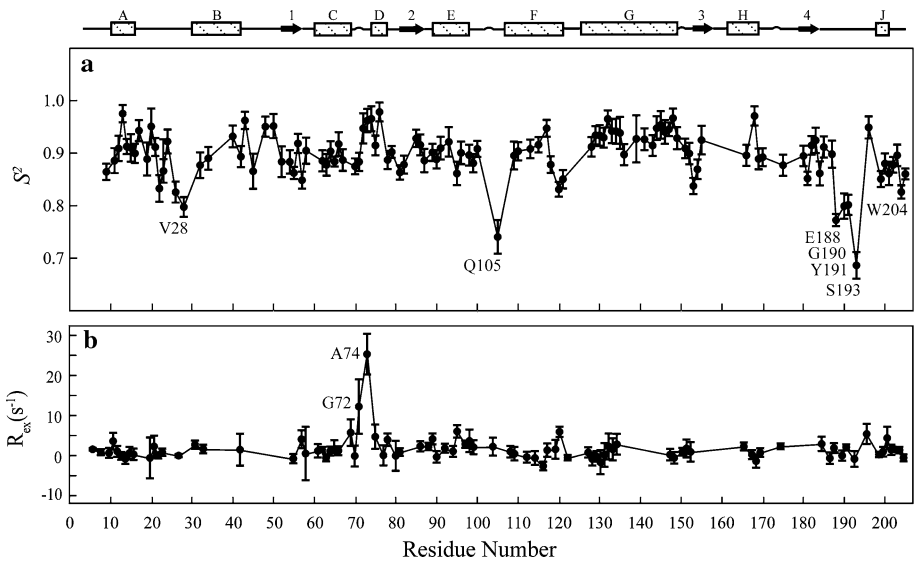

Fig. 5 NOX backbone dynamical parameters, plotted as a function of residue number. **a** Lipari-Szabo order parameters, S^2, reflecting motions on the ns–ps timescale **b** LOSMQ-derived R_{ex} contributions to ^{15}N transverse relaxation, reflecting motions on the ms–μs timescale. In (**a**), labelled residues are those with S^2 less 0.85 at a significance level, $p < 0.05$ ($Z = (0.85 - S^2)/\sigma_S^2 > 1.96$, where σ_S^2 is the uncertainty in S^2)

relaxation rates gives the ^{15}N transverse relaxation rate R_{dd}, which is governed solely by ^{1}H/^{15}N dipole–dipole interactions and is free from R_{ex} contributions. In practice, it is preferable to combine the peak intensities obtained for the four experiments at each relaxation delay (T) into a single parameter, $\beta(T)$ which decays monoexponentially with T as a function of R_{dd} (see Materials and Methods) (Hansen et al. 2007). A representative $\beta(T)$ decay curve obtained for NOX is shown in Fig. 4c. LOSMQ experiments require deuterated protein samples, in order to suppress relaxation pathways involving protons external to the ^{1}H/^{15}N spin pair, therefore we made these measurements on the ^{15}N/^{13}C/^{2}H protein sample. As described above, some amide deuterons did not exchange with solvent protons even after extended high-temperature incubation. Therefore the LOSMQ relaxation data set is smaller than that obtained for traditional spin relaxation experiments performed on a protonated sample, and comprises data for 87 residues. The R_{dd} values are consistent with the R_2 values obtained at 18.8 T, above. In theory, the two rates are expected to be similar but not identical, since they have slightly different dependences on the spectral density function. As expected, the two data sets are close, with an average difference of 0.7 s^{-1} and a root mean squared difference of 3 s^{-1} (excluding data for G72 and A74 as discussed below).

The LOSMQ measurements can be analyzed to yield estimates of the R_{ex} contribution to ^{15}N transverse relaxation remaining under spin-locked conditions (at a field strength of 2 kHz in this case). R_{ex} is negligible for most residues in the protein, with an average value of 1.3 s^{-1} and a standard deviation of 1.8 s^{-1} (excluding data for G72 and A74). Notably, residues G72 and A74, located in the loop between helices C and D, show quite large R_{ex} contributions of 12 and 25 s^{-1} (Fig. 5b), indicating that the ^{15}N chemical shifts of these residues fluctuate on the ms-µs timescale and suggesting that this region of the protein undergoes conformational exchange. Exchange broadening leads to elevated estimates of $J(0)$ (Farrow et al. 1995). The effect increases with increasing spectrometer magnetic field strength, such that $J(0)$ values obtained at 18.8 T are affected to a greater extent than those obtained at 11.7 T. Notably, A74 has the largest value of $\Delta J(0) = J(0)_{18.8T} - J(0)_{11.7T}$ of any residue in the LOSMQ dataset (1.55 ns rad^{-1}). This is consistent with A74 experiencing significant exchange broadening. CPMG pulse sequences (Hansen et al. 2008) can be used to extract quantitative information on exchange processes occurring on the ms–µs timescales. In this case, CPMG dispersion profiles throughout the protein are flat, including those of G72 and A74, implying that the exchange rates for the dynamics are rapid (greater than about 10^4 s^{-1}). Interestingly, R_{dd} values for these two residues are quite low (<10 s^{-1}, compared to an average of 24 s^{-1}), suggesting that they are highly mobile on the ns–ps timescale as well (Fig. 6).

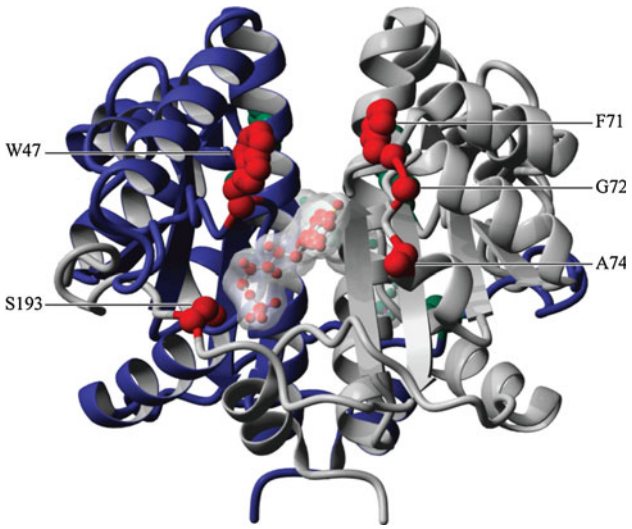

Fig. 6 Structure of NOX, with the two subunits coloured *white* and *blue* and the FMN cofactor illustrated in *ball-and-stick* format with a *semi-transparent molecular surface*. Residues in the two active sites are colored *red* (*in front*) and *green* (*in rear*). Signals for W47 are absent from NMR spectra, likely due to ms–µs dynamical broadening. This residue has previously been proposed to undergo "gating" motions and modulate substrate access to the cofactor. S193 is highly flexible on the ns–ps timescale, and hydrogen bonds with the cofactor. Aromatic residues are conserved at position 71 in homologous proteins. G72 and A74 experience significant ms–µs motions, according to LOSMQ NMR relaxation experiments. Image generated with YASARA View (Krieger et al. 2002)

Discussion

NOX is a thermophilic, dimeric enzyme with structural homology to other flavin reductases and nitroreductases (Hecht et al. 1995; Kobori et al. 2001; Koike et al. 1998; Parkinson et al. 2000; Tanner et al. 1996). Previous studies have implicated protein flexibility as being important in the catalytic mechanism. Addition of urea and other chaotropes at 20°C leads to greater than twofold increases in both k_{cat} and K_m. These changes in activity are accompanied by increased solvent exposure of the active-site residue W47, as evinced by fluorescence quenching measurements and denaturant-dependent changes in near UV circular dichroism spectra (Zoldak et al. 2003, 2004). Conversely, the addition of SO_4^{2-} and other kosmotropes results in decreased values of k_{cat} and K_m and decreased solvent exposure of W47. Further evidence for flexibility in the enzyme mechanism was provided by computer simulations of the enzyme that yielded two different arrangements of the active site, referred to as "open" and "closed" (Hritz et al. 2006). The X-ray crystal structure represents the "open" state in which the side chain of W47 and the FMN

cofactor form a cleft that is large enough to accommodate the NADH substrate. The cleft contains a crystallographic water molecule that hydrogen bonds with a hydroxyl group of FMN and with the backbone amide group of W47. The simulations show excursions to a "closed" conformation in which the W47 side chain moves about 5 Å towards the cofactor, narrowing the cleft and occluding the active site. The water molecule is displaced in this state and the FMN hydroxyl group hydrogen bonds directly with the backbone amide group of W47. In the absence of urea, the protein favours the "closed" form, while introducing urea to the simulation drives the protein towards the "open" state. It was hypothesized that this conformational transition could regulate substrate binding and assist product release by the enzyme.

Notably, a cross-peak has not been identified for the backbone amide group of W47 in $^{1}H/^{15}N$ correlation spectra of NOX. The signals for both adjacent residues have been unambiguously assigned, which strongly suggests that the signal for W47 is absent, rather than just unassigned (Fig. 1). Furthermore, there are only three peaks in the indole region of the spectrum, although each NOX monomer contains four tryptophan residues. As discussed above, the absence of peaks for W47 could be due to either local ms-μs timescale dynamics that broaden its signals beyond detection, or rapid hydrogen exchange with the solvent. The amide groups of the adjacent residues, A46 and N48, are highly protected from *H/D* exchange, producing strong cross-peaks in $^{15}N/^{1}H$ correlation spectra of the protonated sample and no detectable peaks in the deuterated sample as described above. The HNCACB signals obtained for N48 lack inter-residue correlations and the corresponding CBCA(CO)NH peaks are extremely weak. The missing signals would be derived from nuclei in W47, but be detected via the exchange-protected N48 amide group. Thus it appears likely that NMR signals for W47 are strongly attenuated by dynamical broadening rather than by solvent hydrogen exchange. The conformational transition identified in the computer simulations would be expected to produce large changes in the chemical shifts of the both the backbone and indole $^{15}N/^{1}H$ pairs of W47, since it involves remodelling backbone hydrogen bonds, and reorienting the side chain with respect to the aromatic flavin portion of FMN. Thus exchange between the "open" to "closed" forms of the active site occurring on the ms–μs timescales could explain the absence of NMR signals for W47.

In a comparison among structurally homologous flavin reductases and nitroreductases including NOX, it was found that aromatic residues are significantly conserved at three loci in the active sites of these proteins (Hritz et al. 2006). One of these positions covers the middle of the isoalloxazine ring of FMN and corresponds to W47 in NOX. A second conserved aromatic position covers the rim of the pyrimidine ring and corresponds to F71 in NOX. A third conserved aromatic position covers the xylene portion of the FMN ring and corresponds to W131 in NOX. It was noted that aromatic residues frequently serve "gating" roles, regulating access to the active sites of a variety of enzymes. At the first locus, dynamics of W47 are implicated in the function of the enzyme, and its NMR signals are likely broadened beyond detection. Interestingly, at the second locus (F71 in NOX), LOSMQ relaxation experiments indicate that there is extensive dynamical broadening for residues adjacent to F71 (G72 and A74) in the loop between helices *C* and *D*. This raises the interesting possibility that this region of the protein might also be involved in modulating access to the active site, perhaps participating in the same dynamical process as W47.

The Model-Free analysis of ^{15}N relaxation data identified several regions of NOX that are flexible on the ns–ps timescale. Several of these, including the *A–B* and *E–F* loops and the C-terminus, are not close to the active site. Therefore, it is unclear whether these motions could be involved in the catalytic mechanism. Interestingly, the relaxation data also indicate that the long loop between the fourth β-strand and the short C-terminal helix *J* is quite mobile. This sequence forms one edge of the cofactor binding site and helps to coordinate the phospho-ribose portion of the cofactor. In particular, S193, whose side chain hydroxyl proton hydrogen-bonds with the FMN phosphate, has the lowest value of S^2 obtained for any residue in the protein (0.69 ± 0.03). It is somewhat surprising that a residue directly involved in ligand binding should be highly flexible, since tightly interacting residues are often associated with structural rigidity (Jarymowycz and Stone 2006; Kay et al. 1996). One possible role for the flexibility exhibited by this loop is related to the ability of NOX to accept either FMN or FAD as cofactors. It has been proposed that local flexibility on the ns-ps timescale can facilitate larger conformational changes (Clore and Schwieters 2006; Henzler-Wildman et al. 2007). Indeed, the region between E189 and H194, particularly S193, undergoes structural rearrangement when the cofactor FMN is replaced with the larger cofactor FAD, which contains an AMP moiety connected to the ribityl phosphate of FMN (Hecht et al. 1995). We hypothesize that flexibility in the C-terminal phosphate-binding loop may permit rearrangement of the binding site and accommodation of the larger FAD cofactor, and could potentially facilitate other conformational changes occurring within the catalytic cycle. Notably, other structurally homologous flavin reductases and nitroreductases are unable to utilize the FAD cofactor (Hecht et al. 1995; Kobori et al. 2001; Koike et al. 1998; Parkinson et al. 2000; Tanner et al. 1996). Our hypothesis predicts that the active sites of these other enzymes would show less motion on the

ns–ps timescale. NMR dynamical characterization of these related enzymes is an interesting subject for future research.

Conclusion

We have characterized the dynamics of NOX, a 54 kDa dimeric enzyme from *Thermus thermophilus*, using a combination of traditional ^{15}N relaxation and recently-developed LOSMQ NMR spin relaxation experiments. To our knowledge, these are the first NMR studies of an important class of flavin reductase and nitroreductase enzymes with applications in biosensing, pro-drug metabolism and bioremediation. We find that overall, the enzyme has a structurally stable core containing many residues with large *H/D* protection factors, together with a more dynamic periphery with many residues whose signals are absent, due to dynamical broadening and/or solvent hydrogen exchange. One of the residues lacking a detectable signal is W47, located in the active site, whose "gating" motions were previously proposed modulate enzyme activity. The absence of signals for W47 is likely caused by conformational exchange on the ms–μs timescale. The LOSMQ relaxation data indicate the presence of exchange broadening for other residues flanking the active site. Finally, we found that residues in the cofactor phosphate binding site exhibit enhanced ns–ps timescale motions relative to the rest of the protein. Interestingly, the residue exhibiting the largest degree of mobility on the ns–ps timescale donates a hydrogen bond to the cofactor in the X-ray crystal structure. We hypothesize that this flexibility may facilitate structural rearrangement of the active site and the accommodation of different ligands. These results highlight the utility of NMR dynamics methodologies in revealing the molecular basis of protein function.

Acknowledgments This work was funded by grants from the Natural Sciences and Engineering Research Council (NSERC) of Canada and le Fonds Québécois de la Recherche sur la Nature et les Technologies (FQRNT). NMR experiments were recorded at the Québec/Eastern Canada High Field NMR Facility, supported by NSERC, FQRNT and McGill University. The authors thank Prof. Mathias Sprinzl (U. Bayreuth) for the generous gift of the NOX expression plasmid. This paper is dedicated to Prof. Lewis Kay on the occasion of his 50th birthday.

References

Abragam A (1961) Principles of nuclear magnetism. Clarendon Press, Oxford

Amman C, Meier P, Merbach AE (1982) A simple multinuclear NMR thermometer. J Magn Res 46:319–321

Bai YW, Milne JS, Mayne L, Englander SW (1993) Primary structure effects on peptide group hydrogen exchange. Proteins Struct Funct Genet 17:75–86

Best EPH, Kvesitadze G, Khatisashvili G, Sadunishvili T (2005) Plant processes important for the transformation and degradation of explosives contaminants. Z Naturforsch Sect C J Biosci 60:340–348

Brüschweiler R, Liao X, Wright PE (1995) Long-range motional restrictions in a multidomain zinc-finger protein from anisotropic tumbling. Science 268:886–889

Carrasco B, de la Torre JG (1999) Hydrodynamic properties of rigid particles: comparison of different modeling and computational procedures. Biophys J 76:3044–3057

Cho C, Urquidi J, Singh S, Robinson G (1999) Thermal offset viscosities of liquid H_2O D_2O and T_2O. J Phys Chem B 103:1991–1994

Clore GM, Schwieters CD (2006) Concordance of residual dipolar couplings, backbone order parameters and crystallographic B-factors for a small alpha/beta protein: a unified picture of high probability, fast atomic motions in proteins. J Mol Biol 355:879–886

Connelly GP, Bai YW, Jeng MF, Englander SW (1993) Isotope effects in peptide group hydrogen exchange. Proteins Struct Funct Genet 17:87–92

Dachs GU, Tupper J, Tozer GM (2005) From bench to bedside for gene-directed enzyme prodrug therapy of cancer. Anti Cancer Drugs 16:349–359

de la Torre JG, Huertas ML, Carrasco B (2000) HYDRONMR: prediction of NMR relaxation of globular proteins from atomic-level structures and hydrodynamic calculations. J Magn Res 147:138–146

Delaglio F, Grzesiek S, Vuister GW, Zhu G, Pfeifer J, Bax A (1995) NMRPipe: a multidimensional spectral processing system based on UNIX pipes. J Biomol NMR 6:277–293

Englander SW (2000) Protein folding intermediates and pathways studied by hydrogen exchange. Annu Rev Biophys Biomol Struct 29:213–238

Farrow NA, Muhandiram R, Singer AU, Pascal SM, Kay CM, Gish G, Shoelson SE, Pawson T, Forman-Kay JD, Kay LE (1994) Backbone dynamics of a free and phosphopeptide-complexed Src homology 2 domain studied by ^{15}N NMR relaxation. Biochemistry 33:5984

Farrow NA, Zhang OW, Szabo A, Torchia DA, Kay LE (1995) Spectral density-function mapping using ^{15}N relaxation data exclusively. J Biomol NMR 6:153–162

Gardner KH, Kay LE (1998) The use of ^{2}H, ^{13}C, ^{15}N multidimensional NMR to study the structure and dynamics of proteins. Annu Rev Biophys Biomol Struct 27:357–406

Grzesiek S, Bax A (1992) Correlating backbone amide and side chain resonances in larger proteins by multiple relayed triple resonance NMR. J Am Chem Soc 114:6291–6293

Hansen DF, Yang DW, Feng HQ, Zhou Z, Wiesner S, Bai YW, Kay LE (2007) An exchange-free measure of N-15 transverse relaxation: an NMR spectroscopy application to the study of a folding intermediate with pervasive chemical exchange. J Am Chem Soc 129:11468–11479

Hansen AF, Vallurupalli P, Kay LE (2008) An improved N-15 relaxation dispersion experiment for the measurement of millisecond time-scale dynamics in proteins. J Phys Chem B 112:5898–5904

Hansen DF, Feng HQ, Zhou Z, Bai YW, Kay LE (2009) Selective characterization of microsecond motions in proteins by NMR relaxation. J Am Chem Soc 131:16257–16265

Hecht HJ, Erdmann H, Park HJ, Sprinzl M, Schmid RD (1995) Crystal structure of NADH oxidase from *Thermus thermophilus*. Nat Struct Biol 2:1109–1114

Henzler-Wildman KA, Lei M, Thai V, Kerns SJ, Karplus M, Kern D (2007) A hierarchy of timescales in protein dynamics is linked to enzyme catalysis. Nature 450:913–916

Hritz J, Zoldak G, Sedlak E (2006) Cofactor assisted Gating mechanism in the active site of NADH oxidase from *Thermus thermophilus*. Proteins Struct Funct Bioinform 64:465–476

Ikura M, Kay LE, Bax A (1990) A Novel approach for sequential assignment of ^{1}H, ^{13}C and ^{15}N spectra of larger proteins—heteronuclear triple-resonance 3-dimensional NMR spectroscopy—application to calmodulin. Biochemistry 29:4659–4667

Jarymowycz VA, Stone MJ (2006) Fast time scale dynamics of protein backbones: NMR relaxation methods, applications, and functional consequences. Chem Rev 106:1624–1671

Johnson BA, Blevins RA (1994) NMRView: a computer program for the visualization and analysis of NMR data. J Biomol NMR 4:603–614

Kay LE, Muhandiram DR, Farrow NA, Aubin Y, FormanKay JD (1996) Correlation between dynamics and high affinity binding in an SH2 domain interaction. Biochemistry 35:361–368

Kobori T, Sasaki H, Lee WC, Zenno S, Saigo K, Murphy MEP, Tanokura M (2001) Structure and site-directed mutagenesis of a flavoprotein from *Escherichia coli* that reduces nitrocompounds—alteration of pyridine nucleotide binding by a single amino acid substitution. J Biol Chem 276:2816–2823

Koike H, Sasaki H, Kobori T, Zenno S, Saigo K, Murphy MEP, Adman ET, Tanokura M (1998) 1.8 angstrom crystal structure of the major NAD(P)H: FMN oxidoreductase of a bioluminescent bacterium, *Vibrio fischeri*: overall structure, cofactor and substrate-analog binding, and comparison with related flavoproteins. J Mol Biol 280:259–273

Korzhnev DM, Skrynnikov N, Millet O, Torchia DA, Kay LE (2002) An NMR experiment for the accurate measurement of heteronuclear spin-lock relaxation rates. J Am Chem Soc 124:10743–10753

Krieger E, Koraimann G, Vriend G (2002) Increasing the precision of comparative models with YASARA NOVA—a self-parameterizing force field. Proteins Struct Funct Genet 47:393–402

Kurumata M, Takahashi M, Sakamoto A, Ramos JL, Nepovim A, Vanek T, Hirata T, Morikawa H (2005) Tolerance to, and uptake and degradation of 2, 4, 6-trinitrotoluene (TNT) are enhanced by the expression of a bacterial nitroreductase gene in *Arabidopsis thaliana*. Z Naturforsch Sect C J Biosci 60:272–278

Lee LK, Rance M, Chazin WJ, Palmer AG (1997) Rotational diffusion anisotropy of proteins from simultaneous analysis of ^{15}N and $^{13}C\alpha$ nuclear spin relaxation. J Biomol NMR 9:287–298

Lipari G, Szabo A (1982) Model-free approach to the interpretation of nuclear magnetic relaxation in macromolecules: 1. Theory and range of validity. J Am Chem Soc 104:4546–4559

Marley J, Lu M, Bracken C (2001) A method for efficient isotopic labeling of recombinant proteins. J Biomol NMR 20:71–75

Morin S, Gagne SM (2009) Simple tests for the validation of multiple field spin relaxation data. J Biomol NMR 45:361–372

Palmer DH, Chen MJ, Searle PF, Kerr DJ, Young LS (2005) Inhibition of NF-kappa B enhances the cytotoxicity of virus-directed enzyme prodrug therapy and oncolytic adenovirus cancer gene therapy. Gene Ther 12:1187–1197

Park HJ, Kreutzer R, Reiser COA, Sprinzl M (1992) Molecular cloning and nucleotide sequence of the gene encoding a H_2O_2-forming NADH oxidase from the extreme thermophilic thermus-thermophilus HB8 and its expression in *Escherichia coli*. Eur J Biochem 205:875–879

Parkinson GN, Skelly JV, Neidle S (2000) Crystal structure of FMN-dependent nitroreductase from *Escherichia coli* B: a prodrug-activating enzyme. J Med Chem 43:3624–3631

Peng JW, Wagner G (1995) Frequency spectrum of NH bonds in eglin c from spectral density mapping at multiple fields. Biochemistry 34:16733–16752

Saksena MP, Harminder, Kumar S (1975) Viscosity of binary liquid mixtures. J Phys C 8:2376–2381

Serban S, El Murr N (2006) Redox-flexible NADH oxidase biosensor: a platform for various dehydrogenase bioassays and biosensors. Electrochim Acta 51:5143–5149

Tanner JJ, Lei BF, Tu SC, Krause KL (1996) Flavin reductase P: structure of a dimeric enzyme that reduces flavin. Biochemistry 35:13531–13539

Vetterling WT, Press WH, Teukolsky SA, Flannery BR (1988) Numerical recipes in C. Cambridge University Press, Cambridge

Wishart DS, Sykes BD (1994) The ^{13}C chemical shift index—a simple method of the identification of protein secondary structure using ^{13}C chemical shift data. J Biomol NMR 4:171–180

Wittekind M, Mueller L (1993) HNCACB, a high sensitivity 3D NMR experiment to correlate amide proton and nitrogen resonances with the alpha- and beta-carbon resonances in proteins. J Magn Res B 101:201–205

Woessner DE (1962) Nuclear spin relaxation in ellipsoids undergoing rotational Brownian motion. J Chem Phys 37:647–654

Yamazaki T, Lee W, Arrowsmith CH, Muhandiram DR, Kay LE (1994) A suite of triple-resonance NMR experiments for the backbone assignment of ^{15}N, ^{13}C and ^{2}H labeled protein with high sensitivity. J Am Chem Soc 116:11655–11666

Zhang OW, Kay LE, Olivier JP, Formankay JD (1994) Backbone ^{1}H and ^{15}N resonance assignments of the N-terminal SH3 domain of Drk in folded and unfolded states using enhanced-sensitivity pulsed-field gradient NMR techniques. J Biomol NMR 4:845–858

Zoldak G, Sut'ak R, Antalik M, Sprinzl M, Sedlak E (2003) Role of conformational flexibility for enzymatic activity in NADH oxidase from *Thermus thermophilus*. Eur J Biochem 270: 4887–4897

Zoldak G, Sprinzl M, Sedlak E (2004) Modulation of activity of NADH oxidase from *Thermus thermophilus* through change in flexibility in the enzyme active site induced by Hofmeister series anions. Eur J Biochem 271:48–57